Drag reduction properties of superhydrophobic mesh pipes

Nicasio R Geraldi[1]*, Linzi E Dodd[2], Ben B Xu[1], Gary G Wells[1], David Wood[2], Michael I Newton[3] and Glen McHale[1]

[1]Smart Materials and Surfaces Laboratory, Faculty of Engineering & Environment, Northumbria University, Ellison Place, Newcastle upon Tyne, NE1 8ST, United Kingdom.

[2]Microsystems Technology Group, School of Engineering and Computing Sciences, Durham University, South Road, Durham, DH1 3LE, United Kingdom.

[3]School of Science and Technology, Nottingham Trent University, Clifton Lane, Nottingham, NG11 8NS, United Kingdom.

*Corresponding Author.

Email address: nicasio.geraldi@northumbria.ac.uk

Abstract

Even with the recent extensive study into superhydrophobic surfaces, the fabrication of such surfaces on the inside walls of a pipe remains challenging. In this work we report a convenient bi-layered pipe design using a thin superhydrophobic metallic mesh formed into a tube, supported inside another pipe. A flow system was constructed to test the fabricated bi-layer pipeline, which allowed for different constant flow rates of water to be passed through the pipe, whilst the differential pressure was measured, from which the drag coefficient (C_D) and Reynolds numbers (Re) were calculated. Expected values of C_D were found for smooth glass

pipes for the Reynolds number (Re) range 750 to 14000, covering the laminar and part of the turbulent regimes. Flow through plain meshes without the superhydrophobic coating were also measured over this range. After applying the superhydrophobic coating, C_D was found to be less than that of an uncoated mesh, but greater than that of a smooth glass pipe of the same diameter. This demonstrates that a superhydrophobic mesh can support a plastron and provide a drag reduction compared to a plain mesh, however, the plastron is progressively destroyed with use and in particular at higher flow rates.

1. Introduction

When a droplet of water interacts with a surface it exhibits one of two states; it will wet the surface, known as a hydrophilic state, or it will minimise its contact with the surface, known as a hydrophobic state. When a droplet forms a contact angle with the surface of over 150°, and also exhibits low hysteresis between the advancing and receding contact angles, the surface is considered superhydrophobic. Examples of such surfaces in nature include the Lotus leaf which uses the superhydrophobic surface for its self-cleaning properties [1], fire ants which link together to form water repellent rafts [2] and the diving bell spider (*Argyroneta aquatica*) which forms a superhydrophobic layer over its body in water for underwater respiration [3].

Recently there has been great interest in the ability of superhydrophobic surface to produce large area drag reduction. The possibility has been demonstrated using computational fluid dynamics (CFD) simulations [4–13], and experimentally the phenomenon has been demonstrated with the aid of tow tanks [14–16], drop tanks [17–20], circulation [21–24], and rotating plate systems [25,26]. When an object travels through a fluid (external flow), such as

a ship on the ocean, or when a fluid travels through an object (internal flow), such as water through a pipe, there is friction between the fluid and the solid.

An important factor to consider when examining pipe flow is the Darcy friction factor. This was first established in the 1850s by Henry Darcy, and it is a dimensionless quantity that describes the effect of wall roughness on pipe resistance. This friction factor allows for the comparison of pipes with differing dimensions and internal roughness, at different Reynolds numbers, Re, where the Reynolds number is another dimensionless quantity and is the ratio of the inertial and viscous forces.

The use of superhydrophobicity to reduce drag is based on the idea that, on a superhydrophobic surface, the no slip boundary condition is replaced by continuity of shear stress across the various interfaces. The potential for replacing a direct solid-liquid interfacial contact with a solid-vapour followed by a vapour-liquid interface is due to the wetting properties of the solid surface. Two extreme wetting states, the Wenzel [27] and Cassie-Baxter [28] states, exist on rough surfaces. In a Wenzel state a liquid wets the surface and penetrates completely into all surface features. In this state, if a surface material is smooth and hydrophilic, increasing the roughness of the surface will enhance the wetting state and liquids will show stronger wetting tendencies. Conversely, if the surface material is smooth and hydrophobic, increasing the roughness of the surface increases the contact angle and the surface shows stronger hydrophobic tendencies until a critical transition contact angle is met. At this point the liquid no longer retains complete contact with the rough features, but prefers to bridge between the tips of the surface features in a Cassie-Baxter state. With the liquid bridging between the tips of surface features, a layer of air exists between the majority of the solid surface and the liquid. This air layer is called a plastron [29].

The presence of an air layer on an immersed superhydrophobic surface leads to the possibility of a reduction in drag. This is because the no-slip boundary condition is no longer in effect at the liquid/vapour interface, which is present where a solid/liquid interface once existed and an apparent slip can occur [11,19,30]. Air has a much lower viscosity compared to liquids, and so acts to lubricate the flow across a superhydrophobic surface. The lifespan and robustness of the plastron air layer is the limiting factor in the ability of the superhydrophobic surface to demonstrate a reduced drag [31]. Mechanisms by which a plastron can be lost from the surface include diffusion of the gas into the surrounding fluid and the movement of the external liquid stripping the gas layer away. Once the plastron has been destroyed in one area of a surface, the liquid may quickly wet the rest of the rough surface, unless the roughness is tailored to stop the spreading of the wetted area or the plastron is replenished. Recent work in the field has demonstrated such methods [32–35].

To test the effect of superhydrophobic surfaces on internal flows, studies have often concentrated on micro-channels and closely spaced plates, where the modified surface is easily accessible [25,26,36–45]. In 1999, Watanabe *et al* looked at the flow through of water and glycerine solutions through acrylic pipes with and without water repellent walls [46]. They found a 14% reduction in drag in the laminar range (Re<2300). Shirtcliffe *et al* later described how modified copper tubes, with hydrophobic and superhydrophobic internal walls, show increased flow rates for both water and 50% w/w water-glycerol mixtures, at low pressures, below 4 mbar [47]. Walker *et al* have more recently performed flow experiments using modified copper pipes, where they examined the effect of the addition of a superhydrophobic coating on the Reynolds number[48]. More recently, Lv *et al* investigated the flow of water through different diameter aluminium tubes with superhydrophobic internal surfaces for use in

counter-current double-tube heat exchangers [49]. Their experiments did not directly focus on the internal flow in the superhydrophobic tube but did determine that, for this situation, the drag reduction increased with decreasing diameter in the turbulent Re range of 3000 to 11000.

In this article we describe the setup of a constant flow system, the fabrication of a superhydrophobic mesh, and the comparison of *as received* and superhydrophobic stainless steel mesh tubes, tested with water flowing through the pipes over the laminar and turbulent regimes. The use of a mesh provides a conformable micro-structured surface with inherent open voids, where the plain woven wires act as breakers to prevent the progression of plastron collapse. The conformable nature of the material also allows it be installed into an existing pipe section without change to the original tube.

2. Methods

To test the capabilities of a superhydrophobic conformable mesh, the first step was to fabricate pipes from the stainless steel mesh. To begin, (300±1) mm lengths of borosilicate glass pipe (Aimer Products Ltd, UK), with an inner diameter of (7.00±0.15) mm, were cut. Next, strips of #250 stainless steel mesh (SAE304 from The Mesh Company (Warrington) Ltd) were cut, 300 mm x 21.5 mm in dimension. The #250 stainless steel mesh is a plain weave mesh with a wire diameter of (40±2) µm and a wire separation of (65±2) µm. The mesh strips were carefully rolled around a (7±0.15) mm outer diameter rod to form a tubular shape. The mesh tube was then carefully slid inside of the glass tube, whilst making sure the seam of the mesh tube overlapped without buckling. The ends of the mesh were then secured to the tube ends using epoxy resin (Araldite® Rapid).

To render the surface superhydrophobic, the interior of the pipe was coated with Glaco™ Mirror Coat (Nipponshine, UK). This process involves filling the glass/mesh tube with Glaco™, leaving it for 10 s and then pouring out the Glaco™, which is then left for 5 mins for the solvent to evaporate away. The tube is then placed in an oven at 250 °C for 30 mins and subsequently allowed to cool to room temperature. This process was repeated a further two times. The Glaco™ mirror coat is a suspension of silica nanoparticles in alcohol. Overall, we have used a similar process to that of Vakarelski *et al* when they produced superhydrophobic surfaces on steel spheres [50].

To test the tubes with the inserted mesh, a constant flow setup was developed (see Figure 1). Water is constantly pumped at 1000 lph from a large tank of water (100 litres at room temperature) to the constant head tank, which is allowed to overflow back into the large tank. This maintained a constant water level in the head tank, which had to supply a maximum of 225 lph to the test section. The horizontal test section of the setup consisted of an entry pipe, (1.000±0.001) m in length, a test pipe, (0.300±0.001) m in length, and an exit pipe, (0.500±0.001) m in length. All pipe sections were of equivalent material and internal diameter. The entry pipe was made sufficiently long (1000mm) in order for the flow profile to fully develop before entry into the test section. The pipe sections were linked with 10 mm straight couplers to ensure the ends of the pipe were as parallel and as close as possible, without disruption. In order to vary the flow rate, the height between the water level in the constant head tank and the horizontal test section was varied using 3 identical custom stands consisting of horizontal supports every 30 mm along the vertical stand providing a constant flow rate within ±2.5%. The horizontal test section was positioned at 17 different heights below the constant water level ranging from 0.02 m to 1.50 m, which produces a Reynolds number range of 700 to 14000. At each height, 5 measurements of the differential pressure and the mass of

water passing though the test pipe in 30 s to 60 s were recorded. The mass of water collected allowed for the calculation of the mass rate, volumetric flow rate, flow velocity, and the Reynolds number. The temperature of the water, before and after testing, was also recorded. The differential pressure was measured over the length of the test pipe using a digital manometer (Anton APM140) connected to the entry and exit of the test pipe section via a (1.0±0.1) mm diameter hole in the straight coupler. This allowed for the calculation of the Darcy friction factor, C_D.

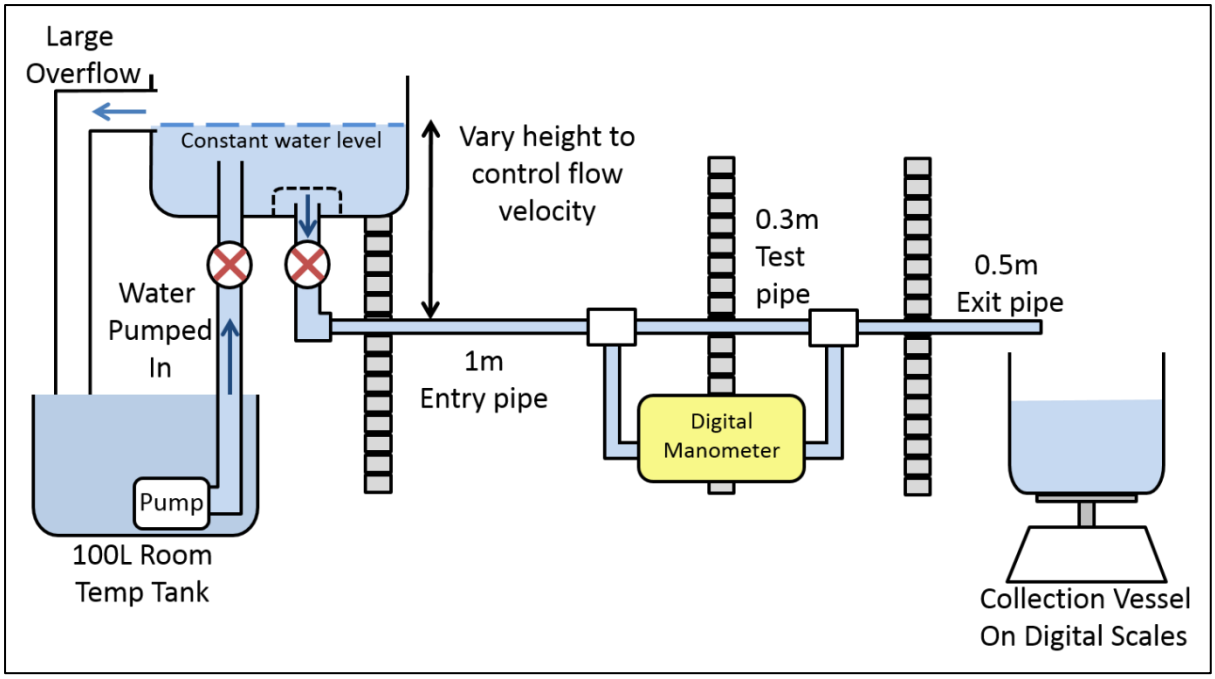

Figure 1. Schematic of the constant flow experimental setup.

SEM images of the uncoated and Glaco™ coated stainless steel mesh are shown in Figure 2, and were taken using a Tescan Mira3 scanning electron microscope. The images show the accumulation of hydrophobic nanoparticles on the surface of the metal wires of the plain weave mesh. The wires of the mesh have a wire diameter of (40±2) µm and are separated by (65±2) µm [51]. Figure 2(a) shows the uncoated stainless steel surface of the mesh. There are few features on the surface of the metal surface apart from the tooling marks left from the

manufacture of the mesh as the metal was drawn. Figure 2(b) shows the state of the metal surface after one round of the coating method. Here we can see small clusters of the sub-50 nm sized nanoparticles evenly distributed over the metallic surface approximately 0.5 μm to 1.0 μm apart.

Figure 2(c) shows the surface after 2 coating processes. The images show how the clusters have grown and the voids are increasingly filled with the nanoparticles. Figure 2(d) are images of the mesh after 2 repetitions of the coating method. The surfaces of the metal wires appear to have a near complete coverage of the nanoparticles. The particles have formed small clusters on the surface and have formed ridges and valleys, all contributing to form a material with 3 scales of roughness, these being the nano-roughness of the particles, the micro-roughness of the cluster formations, and the macro-roughness of the mesh itself.

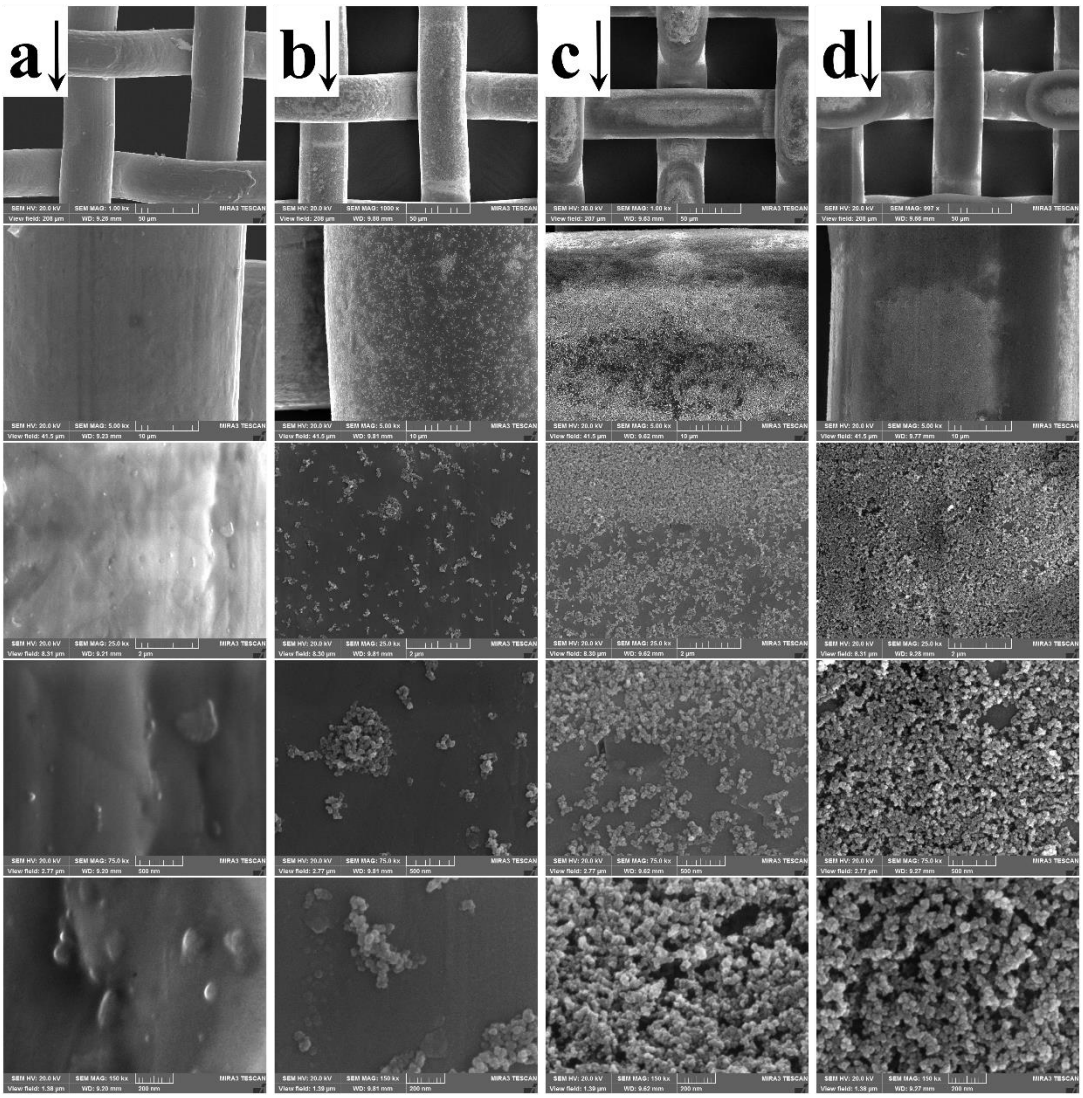

Figure 2. Scanning electron microscopy of the uncoated and Glaco™ coated meshes with increasing magnification down the column, at x1,000, x5,000, x25,000, x75,000, and x150,000 magnifications, respectively. Column (a) shows an uncoated #250 stainless steel mesh and columns (b-d) shows the same mesh after 1 to 3 Glaco™ baking processes, respectively.

To characterise the wetting properties of the surfaces the advancing, receding and static contact angles for the mesh surfaces were measured using a drop shape analysis system (Krüss DSA30). The contact angles were measured a minimum of 3 times on different sample surfaces and an average was calculated. These values are shown in

Table **1**. The flat and mesh stainless steel surfaces show very different contact angles. The advancing contact angle is increased from around (54±1)° to over (135±2)°, respectively, whereas the receding angle decreases from around 12° to approximately 0°, respectively.

Table 1. Contact angles for stainless steel surfaces.

Sample	Number of hydrophobic treatments	Contact angle (°)		
		Static	Advancing	Receding
Flat	0	47.4 ± 0.8	54.3 ± 1.0	11.6 ± 3.9
#250 stainless steel mesh	0	105.2 ± 1.6	135.1 ± 1.6	~0
	1	140.7 ± 1.3	156.2 ± 0.9	93.0 ± 2.0
	2	156.0 ± 1.2	161.7 ± 0.7	144.3 ± 1.2
	3	154.2 ± 1.3	161.9 ± 1.6	149.9 ± 1.5

The application of the Glaco™ coating on the mesh increases the advancing contact angle from ca.135° to over 150° for 3 hydrophobic treatments. There is a larger effect on the receding contact angle, raising it from approximately 0° to around 150° after the third application of the Glaco™ coating (see
Table **1** and Figure 3). These contact angles show that the mesh has low hysteresis after the Glaco™ process and that a Cassie-Baxter state is present.

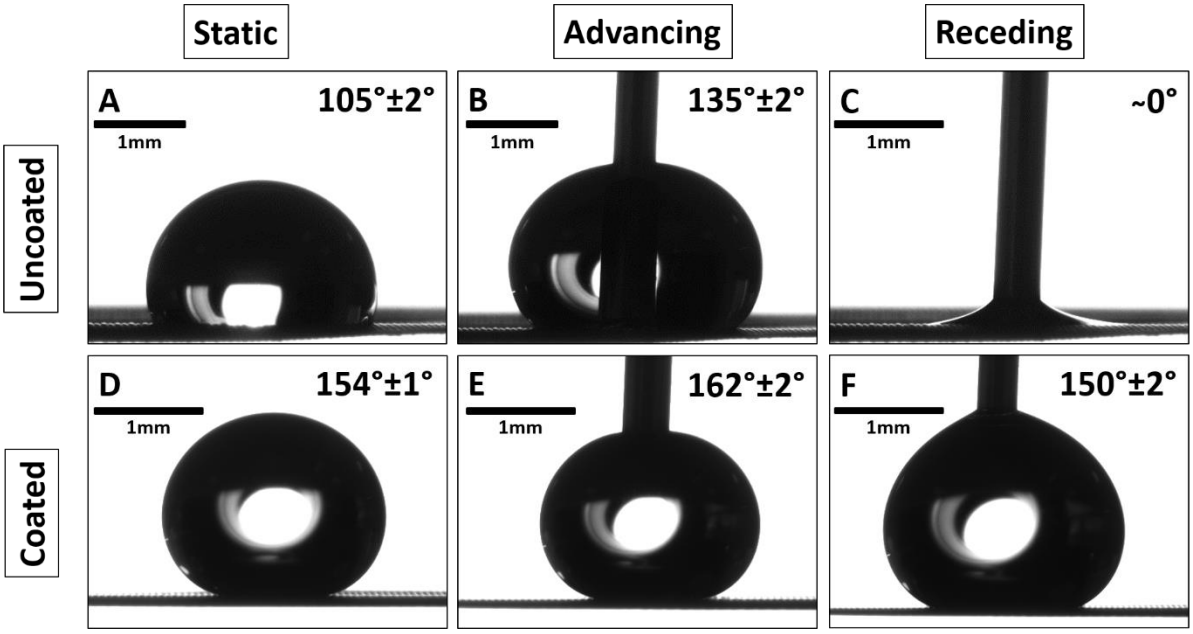

Figure 3. Images of uncoated (A, B, and C) and 3 times Glaco™ coated (D, E, and F) #250 stainless steel mesh.

3. Results and Discussion

In order to compare the different pipes, the friction factor is needed. For the theoretical values, the laminar and turbulent flow regimes were calculated independently. Firstly, the laminar values for the Darcy friction factor were calculated for all values of Re, up to Re=2300, using

$$C_D = \frac{64}{Re} \tag{1}$$

For the turbulent regime the friction factor was calculated using the interpolation formula devised by Colebrook in 1939 to describe turbulent friction [52],

$$\frac{1}{C_D{}^{1/2}} = -4.0 \log_{10}\left(\frac{k_s/2R}{3.7} + \frac{1.26}{ReC_D{}^{1/2}}\right) \tag{2}$$

where k_s is the roughness height and R is the radius of the pipe. Using this equation, the values of Re were found corresponding value of C_D at Re ≥4000.

From the data collected the Reynolds number was calculated using

$$\boldsymbol{Re = \frac{2\rho u R}{\mu}} \tag{3}$$

where ρ is the density of the fluid, u is the flow velocity, and μ is the dynamic viscosity. The friction factor was calculated using

$$\boldsymbol{C_D = \frac{4R(\Delta P)}{\rho u^2 L}} \tag{4}$$

where ΔP is the differential pressure measure over the length (L) of the test pipe [53].

Figure 4 show the data for a glass pipe and an untreated #250 stainless steel test pipe. Data was collected in the range 700≤ Re ≤14000, covering the laminar, transition and turbulent zones. The glass pipe data shows a good agreement with the theoretical line, in both the laminar and turbulent regimes, for a tube of equivalent diameter and with a roughness height of 1.5 µm, equivalent to the roughness height of the glass tube, which was measured using a 3D optical microscope (Bruker Contour GT); this validates the experimental setup.

The experimental data collected for the *as received* #250 stainless steel mesh follows a similar trend to that of the glass pipe in the laminar range, Re ≤2300, but has elevated values in the turbulent range. The results for the #250 mesh pipe shows similar to a theoretical pipe with a roughness height of 60 µm. The plain weave of the material provides a topographical surface with the wires acting as breakers to stop the propagation of plastron-collapse.

Figure 5 shows the data from the superhydrophobic mesh pipe that was tested in the turbulent regime, 4000≤ Re ≤14000 in this case. In order to achieve meaningful results with which to

compare the pipes, we concentrated on the turbulent regime, because accurate and repeatable results in the laminar regime with the constant head setup is challenging. For an increasing flow velocity, the superhydrophobic mesh pipe has a reduced friction factor over the entire range. At R ≈4500, the value of the friction factor is C_D ≈0.039 for the superhydrophobic mesh. This is a fall of approximately 11% from C_D ≈0.044. At the opposite end, Re ≈11000, the fall in the C_D is even greater. The superhydrophobic pipe had a value of C_D ≈0.033 from a value of C_D ≈0.041. This is a 19% reduction in the friction factor, which is due to the presence of the plastron lubricating the flow of water over the surface. The superhydrophobic mesh generates a robust plastron during the increasing flow rate tests as demonstrated by the lowered C_D over the turbulent range tested, that does not appear to be stripped from the surface by the flowing water.

For the same superhydrophobic pipe tested with a decreasing flow rate, its initial friction factor at the start of the test was similar to that of the final results of the increasing flow rate tests, with C_D ≈0.033. But unlike the increasing flow rate tests, the friction factor for decreasing flow rate did not remain as low, and rises significantly after the initial test flow rate at Re =10960. The friction factor increases, going from 0.033 to 0.035. Over the range, 4000< Re <12000, the decreasing Re test had a friction factor ~0.02 higher than the increasing Re test. Even with a higher C_D than during the increasing Re tests, the hydrophobised mesh still has a lower friction factor in the decreasing flow rate tests than it did with an unprocessed surface. The reduction in the ability of the surface to reduce drag in the decreasing case may be due to the pressure exerted by the flow on the plastron. When the flow rate starts low and increases, the pressure generated in the pipe steadily increases, exerting more pressure on the plastron and the surface of the mesh as the flow rate increases, with the maximum force being exerted at the end of the test. Only at this point is the maximum damage caused to the plastron. When

performing the test with a decreasing flow rate the plastron is damaged at the onset of the test and is not able to recover, and this in turn leads to a diminished drag reduction.

Figure 5 shows the results for flow tests performed from a starting Reynolds number of approximately 5000. The tests determined the friction factor of the superhydrophobic mesh pipe as the flow rate was increased or decreased from the starting point. The decreasing test shows that the friction remained low, equivalent to that of a smooth pipe and a superhydrophobic mesh pipe tested for an increasing flow rate over $4000 < Re < 6000$. For the increasing test, the friction factor measured from the pressure drop, is elevated and shows similarity to that of the superhydrophobic mesh pipe tested with a decreasing flow rate.

All sets of superhydrophobic pipe data show a reduced drag in the pipe when compared to the untreated mesh, but at no point presented a friction factor less than that of a smooth pipe. The data demonstrates that a superhydrophobic mesh pipe has a lower friction factor than that of a plain mesh pipe due to the presence of the plastron, but the plastron is slowly stripped from the interior surface of the tubes in the turbulent flow and the drag reduction is diminished.

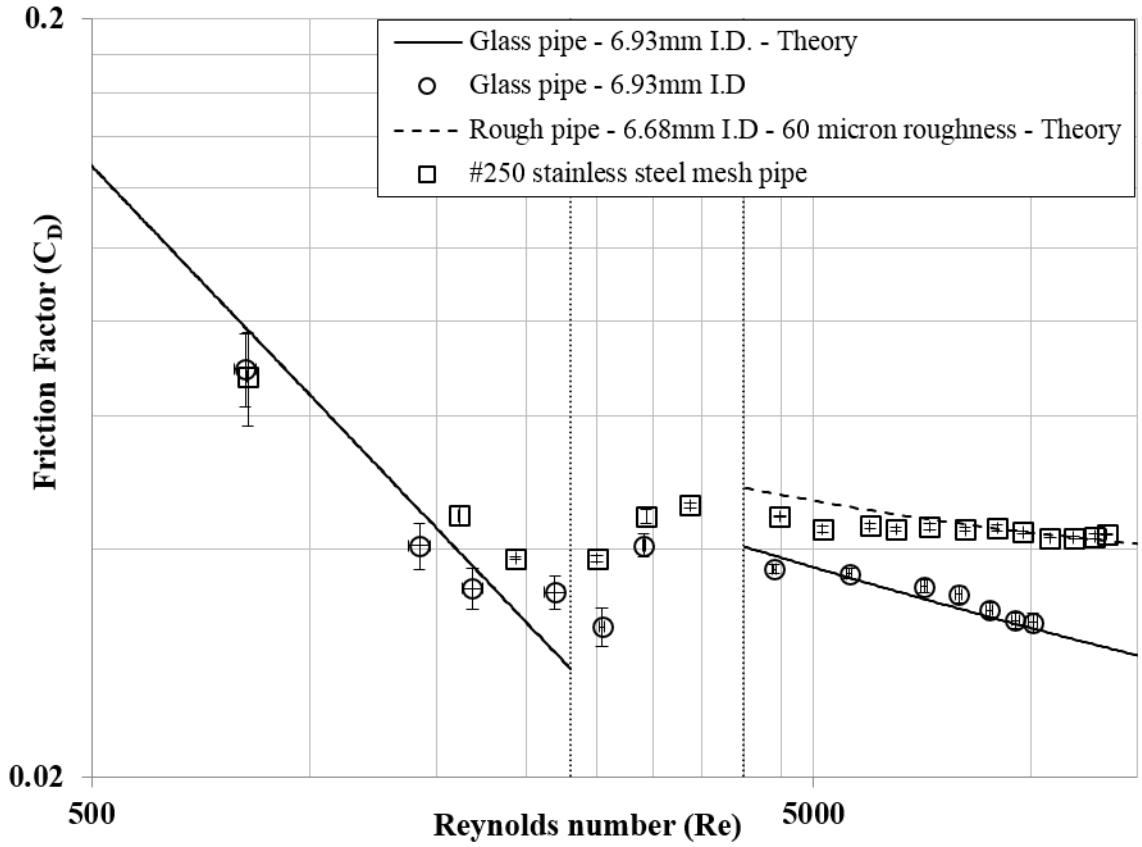

Figure 4. The friction factor (C_D) at different Reynolds number (Re) for a theoretical glass pipe (—), an experimental glass pipe (○), a theoretical pipe with 60 micron roughness (---), and a #250 stainless steel mesh pipe (□).

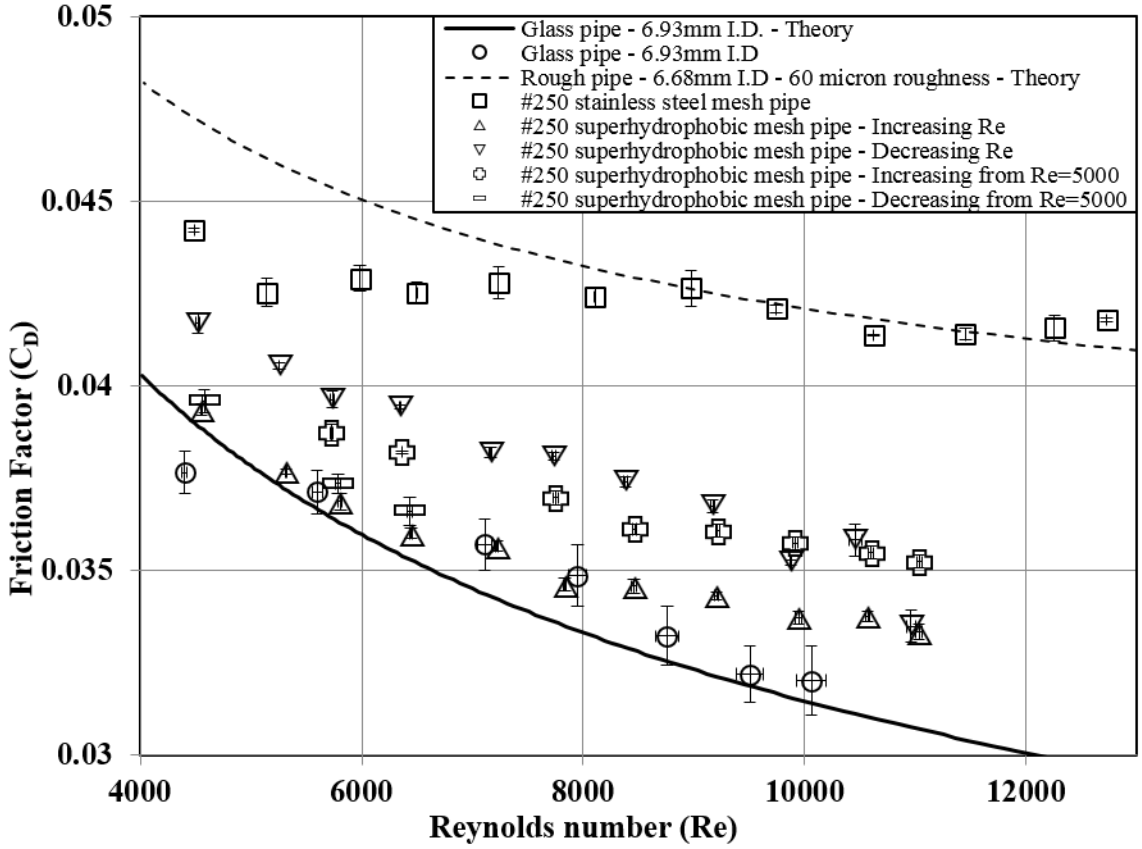

Figure 5. The friction factor (C_D) at different Reynolds number (Re) for a theoretical pipe with 60 μm roughness (dashed line), a #250 stainless steel mesh pipe (□), a 3 times Glaco™ treated #250 stainless steel mesh tested with increasing (Δ) and decreasing (**∇**) Re, and a 3 times Glaco™ treated #250 stainless steel mesh tested from Re ≈5000 upward (□) and Re ≈5000 downwards (▭).

4. Conclusion

In this work we have shown it is possible to construct a flow system from which the mass flow rate at pressure data equivalent to the expected values for Darcy friction factor can be captured, for smooth glass pipes in the Reynolds number range 750 to 14000. A simple technique has been demonstrated for producing superhydrophobic mesh pipes and the friction factors for these have been found over the same Re range. After the application of the superhydrophobic coating, C_D was found to be less than that of an uncoated mesh, but greater than that of a smooth glass pipe of the same diameter. This demonstrates that a superhydrophobic mesh can support a plastron and provide a drag reduction compared to a plain mesh, however, the plastron is progressively destroyed with use and in particular at high flow rates.

5. Acknowledgements

Funding from the UK Engineering and Physical Sciences Research Council (EPSRC) under grants EP/L026899/1, EP/L026341/1 and EP/L026619/1 is gratefully acknowledged. The authors would also like to thank Professor James Martin and Dr Simone Stuart-Cole from Reece Innovation, Newcastle upon Tyne, and Professor Christopher Underwood for their input and guidance.

6. References

[1] Barthlott W and Neinhuis C 1997 Purity of the sacred lotus, or escape from contamination in biological surfaces *Planta* **202** 1–8

[2] Mlot N J, Tovey C A and Hu D L 2011 Fire ants self-assemble into waterproof rafts to survive floods *Proceedings of the National Academy of Sciences* **108** 7669–73

[3] Shirtcliffe N J, McHale G, Newton M I, Perry C C and Pyatt F B 2006 Plastron properties of a

superhydrophobic surface *Applied Physics Letters* **89** 104106

[4] Min T and Kim J 2004 Effects of hydrophobic surface on skin-friction drag *Physics of Fluids* **16** 55–9

[5] Fukagata K, Kasagi N and Koumoutsakos P 2006 A theoretical prediction of friction drag reduction in turbulent flow by superhydrophobic surfaces *Physics of Fluids* **18** 51703

[6] Busse A and Sandham N D 2012 Influence of an anisotropic slip-length boundary condition on turbulent channel flow *Physics of Fluids* **24** 55111

[7] Gruncell B R K, Sandham N D and McHale G 2013 Simulations of laminar flow past a superhydrophobic sphere with drag reduction and separation delay *Physics of Fluids* **25** 43601

[8] Busse A, Sandham N D, McHale G and Newton M I 2013 Change in drag, apparent slip and optimum air layer thickness for laminar flow over an idealised superhydrophobic surface *Journal of Fluid Mechanics* **727** 488–508

[9] Tsekov R and Radoev B 1999 Surface forces and dynamic effects in thin liquid films on solid interfaces *International Journal of Mineral Processing* **56** 61–74

[10] Vinogradova O I 1995 Drainage of a Thin Liquid Film Confined between Hydrophobic Surfaces *Langmuir* **11** 2213–20

[11] Rothstein J P 2010 Slip on Superhydrophobic Surfaces *Annual Review of Fluid Mechanics* **42** 89–109

[12] Vinogradova O I and Dubov A L 2012 Superhydrophobic Textures for Microfluidics *Mendeleev Communications* **22** 229–36

[13] Legendre D, Lauga E and Magnaudet J 2009 Influence of slip on the dynamics of two-dimensional wakes *Journal of Fluid Mechanics* **633** 437

[14] Dong H, Cheng M, Zhang Y, Wei H and Shi F 2013 Extraordinary drag-reducing effect of a superhydrophobic coating on a macroscopic model ship at high speed *Journal of Materials Chemistry A* **1** 5886

[15] Aljallis E, Sarshar M A, Datla R, Sikka V, Jones A and Choi C-H 2013 Experimental study of skin friction drag reduction on superhydrophobic flat plates in high Reynolds number boundary layer flow *Physics of Fluids* **25** 25103

[16] Zhang S, Ouyang X, Li J, Gao S, Han S, Liu L and Wei H 2015 Underwater drag-reducing effect of superhydrophobic submarine model *Langmuir* **31** 587–93

[17] McHale G, Shirtcliffe N J, Evans C R and Newton M I 2009 Terminal velocity and drag reduction measurements on superhydrophobic spheres *Applied Physics Letters* **94** 64104

[18] McHale G, Flynn M R and Newton M I 2011 Plastron induced drag reduction and increased slip on a superhydrophobic sphere *Soft Matter* **7** 10100

[19] McHale G, Newton M I and Shirtcliffe N J 2010 Immersed superhydrophobic surfaces: Gas exchange, slip and drag reduction properties *Soft Matter* **6** 714

[20] Brassard J D, Sarkar D K and Perron J 2015 Studies of drag on the nanocomposite superhydrophobic surfaces *Applied Surface Science* **324** 525–31

[21] Muralidhar P, Ferrer N, Daniello R and Rothstein J P 2011 Influence of slip on the flow past superhydrophobic circular cylinders *Journal of Fluid Mechanics* **680** 459–76

[22] Daniello R, Muralidhar P, Carron N, Greene M and Rothstein J P 2013 Influence of slip on vortex-induced motion of a superhydrophobic cylinder *Journal of Fluids and Structures* **42** 358–68

[23] Brennan J C, Fairhurst D J, Morris R H, McHale G and Newton M I 2014 Investigation of the drag reducing effect of hydrophobized sand on cylinders *Journal of Physics D: Applied Physics* **47** 205302

[24] Brennan J C, Geraldi N R, Morris R H, Fairhurst D J, McHale G and Newton M I 2015 Flexible conformable hydrophobized surfaces for turbulent flow drag reduction *Scientific Reports* **5** 10267

[25] Srinivasan S, Choi W, Park K-C, Chhatre S S, Cohen R E and McKinley G H 2013 Drag reduction for viscous laminar flow on spray-coated non-wetting surfaces *Soft Matter* **9** 5691

[26] Truesdell R, Mammoli A, Vorobieff P, Swol F Van and Brinker C J 2006 Drag Reduction on a Patterned Superhydrophobic Surface **44504** 1–4

[27] Wenzel R N 1936 Resistance Of Solid Surfaces To Wetting By Water *Industrial & Engineering Chemistry* **28** 988–94

[28] Cassie A B D and Baxter S 1944 Wettability of porous surfaces *Transactions of the Faraday Society* **40** 546

[29] Shirtcliffe N J, McHale G, Newton M I, Perry C C and Pyatt F B 2006 Plastron properties of a superhydrophobic surface *Applied Physics Letters* **89** 104106

[30] de Gennes P G 2002 On Fluid/Wall Slippage *Langmuir* **18** 3413–4

[31] Samaha M A, Tafreshi H V and Gad-El-Hak M 2012 Influence of flow on longevity of superhydrophobic coatings *Langmuir* **28** 9759–66

[32] Vakarelski I U, Chan D Y C, Marston J O and Thoroddsen S T 2013 Dynamic air layer on textured superhydrophobic surfaces. *Langmuir : the ACS journal of surfaces and colloids* **29** 11074–81

[33] Lee C and Kim C-J 2011 Underwater Restoration and Retention of Gases on Superhydrophobic Surfaces for Drag Reduction *Physical Review Letters* **106** 14502

[34] Vakarelski I U, Patankar N a, Marston J O, Chan D Y C and Thoroddsen S T 2012 Stabilization of Leidenfrost vapour layer by textured superhydrophobic surfaces *Nature* **489** 274–7

[35] Golovin K B, Gose J W, Perlin M, Ceccio S L and Tuteja A 2016 Bioinspired surfaces for turbulent drag reduction *Philosophical Transactions of the Royal Society of London A: Mathematical, Physical and Engineering Sciences* **374**

[36] Ou J, Perot B and Rothstein J P 2004 Laminar drag reduction in microchannels using ultrahydrophobic surfaces *Physics of Fluids* **16** 4635

[37] Ou J and Rothstein J P 2005 Direct velocity measurements of the flow past drag-reducing ultrahydrophobic surfaces *Physics of Fluids* **17** 1–10

[38] Joseph P, Cottin-Bizonne C, Benoît J-M, Ybert C, Journet C, Tabeling P and Bocquet L 2006 Slippage of Water Past Superhydrophobic Carbon Nanotube Forests in Microchannels ed Intergovernmental Panel on Climate Change *Physical Review Letters* **97** 156104

[39] Daniello R J, Waterhouse N E and Rothstein J P 2009 Drag reduction in turbulent flows over

superhydrophobic surfaces *Physics of Fluids* **21** 85103

[40] Choi C-H and Kim C-J 2006 Large Slip of Aqueous Liquid Flow over a Nanoengineered Superhydrophobic Surface *Physical Review Letters* **96** 66001

[41] Lee C, Choi C-H and Kim C-J 2008 Structured Surfaces for a Giant Liquid Slip *Physical Review Letters* **101** 64501

[42] Ahmmed K M T, Patience C and Kietzig A-M 2016 Internal and External Flow over Laser-Textured Superhydrophobic Polytetrafluoroethylene (PTFE) *ACS Applied Materials & Interfaces* **8** 27411–9

[43] Rosenberg B J, Van Buren T, Fu M K and Smits A J 2016 Turbulent drag reduction over air- and liquid- impregnated surfaces *Physics of Fluids* **28** 15103

[44] Ling H, Srinivasan S, Golovin K, Mckinley G H, Tuteja A and Katz J 2016 High-resolution velocity measurement in the inner part of turbulent boundary layers over super-hydrophobic surfaces *J. Fluid Mech* **801** 670–703

[45] Kavalenka M N, Vüllers F, Lischker S, Zeiger C, Hopf A, Röhrig M, Rapp B E, Worgull M and Hölscher H 2015 Bioinspired Air-Retaining Nanofur for Drag Reduction *ACS Applied Materials and Interfaces* **7** 10651–5

[46] Watanabe K, Udagawa Y and Udagawa H 1999 Drag reduction of Newtonian fluid in a circular pipe with a highly water-repellent wall *Journal of Fluid Mechanics* **381** 225–38

[47] Shirtcliffe N J, McHale G, Newton M I and Zhang Y 2009 Superhydrophobic Copper Tubes with Possible Flow Enhancement and Drag Reduction *ACS Applied Materials & Interfaces* **1** 1316–23

[48] Walker G M, Albadarin A B, McGlue A, Brennan S and Bell S E J 2014 Analysis of friction factor reduction in turbulent water flow using a superhydrophobic coating *Progress in Organic Coatings* **90** 472–6

[49] Lv F Y and Zhang P 2016 Drag reduction and heat transfer characteristics of water flow through the tubes with superhydrophobic surfaces *Energy Conversion and Management* **113** 165–76

[50] Vakarelski I U 2012 Stabilization of Leidenfrost vapour layer by textured superhydrophobic surfaces - Supplementary information *Nature*

[51] Geraldi N R, McHale G, Xu B B, Wells G G, Dodd L E, Wood D and Newton M I 2016 Leidenfrost transition temperature for stainless steel meshes *Materials Letters* **176** 205–8

[52] Colebrook C F, Blench T, Chatley H, Essex E H, Finnecome J R, Lacey G, Williamson J and Macdonald G G 1939 Turbulent Flow in Pipes, with Particular Reference to the Transition between the Smooth and Rough Pipe Laws *Journal of the Institution of Civil Engineers* **12** 393–422

[53] McHale G 2017 CHAPTER 9. Wetting Properties of Surfaces and Drag Reduction *Non-wettable Surfaces* ed R H A Ras and A Marmur (Cambridge: Royal Society of Chemistry) pp 253–84